Composites: Part A 40 (2009) 613–624

Contents lists available at ScienceDirect

Composites: Part A

journal homepage: www.elsevier.com/locate/compositesa

An experimental and numerical investigation into the damage mechanisms in notched composites

S.R. Hallett *, B.G. Green [1], W.G. Jiang [2], M.R. Wisnom

Advanced Composites Centre for Innovation and Science, University of Bristol Queens Building, University Walk, Bristol BS8 1TR, UK

ARTICLE INFO

Article history:
Received 7 November 2008
Received in revised form 3 February 2009
Accepted 14 February 2009

Keywords:
A. Carbon fibre
C. Finite element analysis (FEA)
D. Mechanical testing

ABSTRACT

Investigations of the effect of size on the tensile strength of composite laminates containing circular holes show that there is a large difference both in failure stress and mechanism due to changes in test configuration. This is particularly true of the ply and laminate thickness, and hole diameter. Interrupted tests have been performed on open hole tensile specimens at different load levels to determine the progressive damage development, evaluated through non-destructive testing (X-ray and C-scanning). The tests were also analysed using a novel Finite Element Modelling technique. This was able to accurately predict the wide range of ultimate strengths measured with variation in test parameters, principally through incorporation of the sub-critical damage in the analysis. A significant damage mechanism was seen to be delamination at the hole edge which generally occurred at a lower stress for a smaller hole diameter to ply block thickness ratio. Delaminations allowed damage to join up through the thickness of the laminate and propagate. In ply-level scaled specimens, the delamination propagation was the ultimate failure mode of most of the specimens. In sub-laminate level scaled specimens, localised damage relieved stress in the 0° fibres at the hole edge, delaying the onset of fibre failure. Less damage was seen for larger holes, thus leading to a decreasing failure stress with increasing hole diameter.

1. Introduction

The scaling effect and notched behaviour of composite materials has been investigated in detail over the past 30 years, in both experimental and modelling programs. As the size and structural importance of composite components have increased recently, so the understanding of the extent of the size effect present in composite materials, the mechanisms behind it, and the ability to accurately account for it during the design process have become increasingly important areas of research [1].

Early work in the field, as summarised by Awerbuch and Madhukar [2], focussed on understanding the effect from a global point of view. For hole diameters under 25 mm, a deviation in the tensile strength from the unnotched strength divided by the stress concentration factor was noted. Predictive methods for notched strength were based on the experimental programs performed, resulting, for example, in the average stress criterion of Whitney and Nuismer [3] which uses an empirical parameter to account for the change in mechanical behaviour with hole size.

In their review, Awerbuch and Madhukar suggested that notch sensitivity must be determined by the damage occurring at the notch edge. Subsequent work has focussed on understanding this damage occurring at the notch, including this in damage progression models that predict the damage occurring prior to failure, and accounting for its effect on mechanical behaviour. Various authors have conducted detailed experimental research into the damage mechanisms occurring in notched composites. Chang and Chang [4] produced one of the first damage progression models, taking account of in-plane damage mechanisms. The damage patterns and mechanical behaviour predicted for $(0/\pm 45/90)_{2s}$ specimens was similar to that observed experimentally, where damage initiated through matrix cracking in the 90° plies before propagating through the 45° plies. When the cracking reached the 0° plies, failure followed by fibre rupture. Failure in $(0_2/\pm 45)_{2s}$ specimens occurred through fibre-matrix shearing and fibre breakage.

Kortschot and Beaumont [5–7] developed a numerical model [5] based on the shape of the damage zones observed in $(0_n/90_n)_{ns}$ graphite/epoxy specimens [6]. The damage was predicted using a 2-layer finite element (FE) model, with delamination damage directly embedded through coincident nodes and fibre failure based on a Weibull stress analysis [7]. The experimental strength and damage zone size at failure correlated well with the predictions. Hallett and Wisnom [8] carried out a similar experimental investigation using glass/epoxy specimens, extending it to

* Corresponding author. Tel.: +44 117 331 7098; fax: +44 117 927 2771.
E-mail address: stephen.hallett@bristol.ac.uk (S.R. Hallett).
[1] Present address: Gurit UK, St Cross Business Park, Newport, Isle of Wight PO30 5WU, UK.
[2] Present address: School of Mechanical Engineering, Yanshan University, Qinhuangdao, PR China.

1359-835X/$ - see front matter © 2009 Elsevier Ltd. All rights reserved.
doi:10.1016/j.compositesa.2009.02.021

quasi-isotropic laminates. This tracked in considerable detail the development of the damage in the form of splits emanating from the notch tip and their associated delaminations.

Numerical models such as those presented by Chang and Chang [4] and others [9,10] do not take account of this delamination between the plies. More recent numerical models have started to use cohesive interface elements to model the sub-critical damage which occurs at the notch tip [11–14]. These are able to account for the local damage occurring at the point of stress concentration which in turn alters the magnitude of that stress concentration, thus affecting ultimate failure. Most of these detailed models have however not managed to combine the local damage development and global ultimate failure prediction.

A previous experimental investigation by the authors [15] comprehensively investigated the effect of specimen size for open hole tensile tests. This varied the thickness, in-plane dimensions and full 3D scaling. It also looked at the variations in strength obtained with two thickness scaling methods, either blocking plies of the same orientation together or using multiple blocks of sub-laminates. The current paper is focussed on further experimental work on interrupted tests to capture in detail the process by which the damage develops in such specimens. This has informed development of finite element models to predict the failure of the specimens. The prediction of this damage is included in models through the use of cohesive interface elements [16]. When combined with a statistically based fibre failure criterion it is able to very successfully predict the full range of scaling effects for open hole tension tests presented in [15].

2. Tensile strength experimental results

The previously published experimental results [15] cover an extensive program investigating the extent of the size effect on open hole tensile strength. Quasi-isotropic $[45/90/-45/0]_s$ carbon fibre/epoxy (IM7/8552) specimens with a centrally located circular hole were tested in tension. Specimens were scaled from the baseline specimen size by a factor of 2 each time, up to a maximum of 8. Three different scaling routines were used: 1D, where only the specimen thickness was increased; 2D, where in-plane dimensions (specimen length, width, and hole diameter) were increased; and 3D, where all dimensions were simultaneously increased. The increase in specimen thickness was achieved in two ways: sub-laminate level scaling, where the basic sub-laminate is repeated as often as is required ($[45/90/-45/0]_{ns}$); and ply-level scaling, where plies of the same orientation are stacked together to increase the effective ply thickness ($[45_n/90_n/-45_n/0_n]_s$). Results from this testing programme are summarised in Table 1.

In each case a load drop of 5% on the load–displacement curve was taken to represent specimen failure. As well as the differences in strength, there were three distinct failure mechanisms observed in the testing program, termed pull-out, brittle and delamination, as shown in the Table. The brittle failure mechanism was dominated by fibre failure with little evidence of delamination and the failed specimens were characterised by a relatively clean break across the width, perpendicular to the direction of loading (Fig. 1a).The pull-out failure mechanism was also dominated by fibre breakage but this was characterised by large amounts of delamination and ply cracking, such that the off axis plies were able to "pull-out" from the adjacent plies, giving the characteristic failure pattern shown in Fig. 1b. In the case of the delamination failure mode, fibre failure was not always present. At failure a significant delamination propagated back from the hole to the gripping region at the $-45/0^\circ$ interface, causing a load drop greater than 5%. Whilst the remaining 0° could carry some load, the specimen had to all intents and purposes lost structural integrity and could be deemed to have failed.

Table 1
Experimental strength results (MPa) for scaled open hole tensile tests [15].

Laminate thickness t (mm)	Hole sizes (mm)							
	Sub-laminate level scaling				Ply-level scaling			
	3.175	6.35	12.7	25.4	3.175	6.35	12.7	25.4
1	**570**				**570**			
2	**500**	*438*			396	**498**[a]		
4	**478**	*433*	*374*	*331*	275	285	362	417
8	**476**			*332*	202			232

Bold font values indicate pull-out, italicized values indicate brittle, and underlined values indicate delamination type failures.

[a] Multiple failure modes were observed within this series of tests but the dominant one is pull-out.

3. Interrupted tests

Selected tests from the full experimental program from [15] were repeated using virgin specimens and interrupted at pre-determined load levels prior to failure. 4 mm thick specimens with hole diameters of 3.175, 6.35, 12.7 and 25.4 mm were tested for sub-laminate level scaled specimens and 3.175, 6.35 and 12.7 mm hole diameters for ply-level scaled specimens. A plan view of the specimen geometry is shown in Fig. 2. All specimens had cross-ply glass–epoxy tabbing of length 50 mm. Sub-laminate level scaled specimens were interrupted at 40, 70 and 95% of their nominal failure load (one for each hole size at each load level). Ply-level scaled specimens were interrupted at 40, 60, 80 and 95% of their nominal failure load. The nominal stresses at which loading of the different specimen sizes was stopped are given in Table 2, as determined from the previous testing program. The specimens were all loaded at displacement rates equivalent to a constant strain rate of 0.5%/ min.

After stopping the loading at the prescribed stress level, the specimens were examined via X-radiography and C-scanning to assess their damage development. The specimens for X-ray were first soaked in a bath of zinc–iodide dye-penetrant. Specimens for C-scanning were immersed in a water bath, and scanned at a rate of 2 mm/s, with a resolution of 0.25 mm.

4. Experimental results – damage growth

The interrupted test programme described above has been able to characterise typical damage development sequences for both sub-laminate and ply-level scaled specimens. Below, the damage is explained for a generic $[45/90/-45/0]_s$ laminate, with any differences between sub-laminate and ply-level scaled specimens highlighted.

The damage can be divided into four separate stages, according to its location in the specimen, as shown schematically in Fig. 3, occurring in the following order:

1. Isolated damage at the hole and specimen free edge;
2. Interconnected damage at the hole (inner delamination regions) and localised damage at the free edge resulting from full width matrix cracks;
3. Damage across the width of the specimen in a "zone of influence" of the hole, i.e. the outer delamination regions, bounded by + and -45° cracks emanating from the hole; and
4. Final catastrophic failure.

The extent of damage at each of the different stages varied quite considerably with ply thickness and scaling methodology. The stress levels at which each stage occurred relative to the fibre failure stress resulted in the different failure modes already identified. In the brittle failure mode stages 2 and 3 were not present.

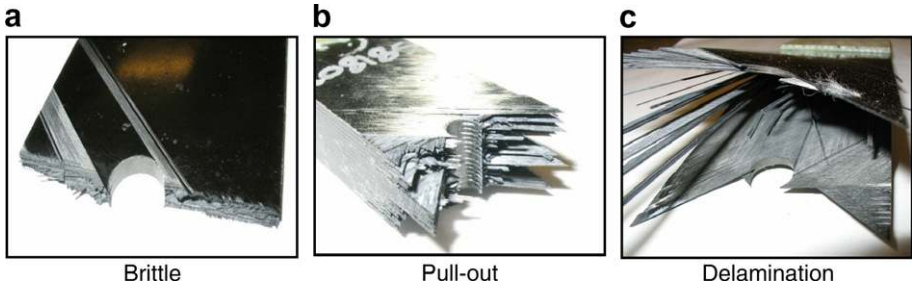

Fig. 1. Three different failure mechanisms observed depending on scaling regime and specimen dimensions (see Table 1).

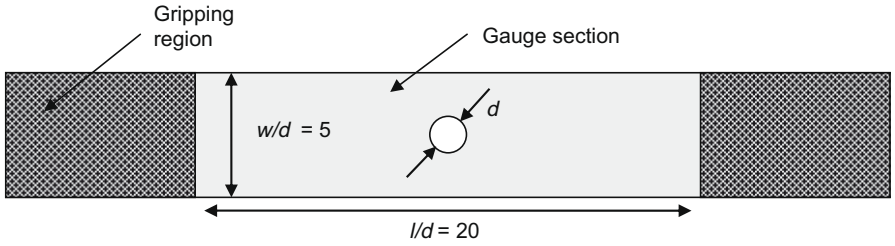

Fig. 2. Specimen configuration.

Table 2
Stress levels for interrupted testing program (MPa).

% Static load at interruption	Hole sizes (mm)							
	Sub-laminate level scaling				Ply-level scaling			
	3.175	6.35	12.7	25.4	3.175	6.35	12.7	25.4
40	191	173	150	132	110	114	145	
60					165	171	217	
70	335	303	262	232				
80					220	228	290	
95	454	411	355	314	261	271	344	

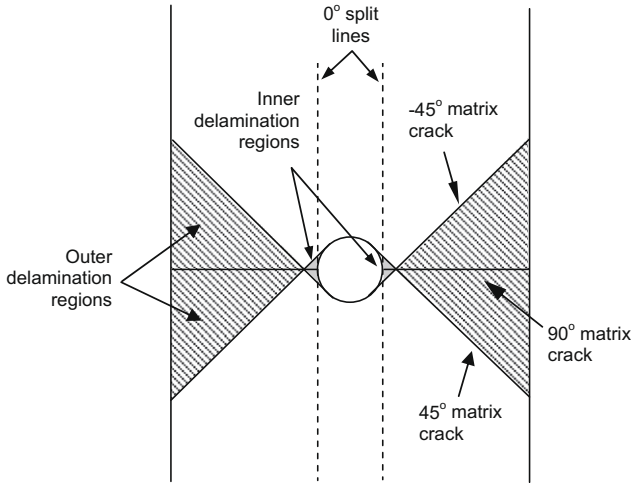

Fig. 3. Damage zones associated with $[45/90/-45/0]_s$ specimens.

The first failure observed in the laminates was matrix cracking in the 90° plies at the hole boundary. This was followed by isolated matrix cracks occurring in the off-axis plies, within the bounds of the inner delamination regions in the surface plies. All of the matrix cracks in the off axis plies were accompanied by small local delaminations at the adjacent interfaces. These occurred in an almost triangular pattern between the cracks and the hole edge, of a size similar in magnitude to the ply thickness. Such delaminations at the intersection of a matrix crack and free edge have been reported in the literature previously [17], and are a result of the high interlaminar normal and shear stresses occurring there. These failure mechanisms can be seen in the X-ray image of a ply-level scaled specimen with a 12.7 mm diameter hole loaded to 40% of its ultimate stress (Fig. 4).

In the second stage of damage development, the isolated cracks, splits and associated delaminations join together to cover the inner delamination region, as shown in Fig. 5a. The delaminations initiated at the interface nearest to the surface of the laminate and propagated through the thickness by stepping down through matrix cracks within the adjacent plies, although in the sub-laminate level scaled specimens the delamination propagation through the full thickness was obstructed by the 0° ply closest to the surface, through which it could not pass without breaking fibres since it does not contain any full width matrix cracks. Plies clearly pulled apart from each other at the hole edge, and cracks were visible through the thickness of plies where the delamination passed from

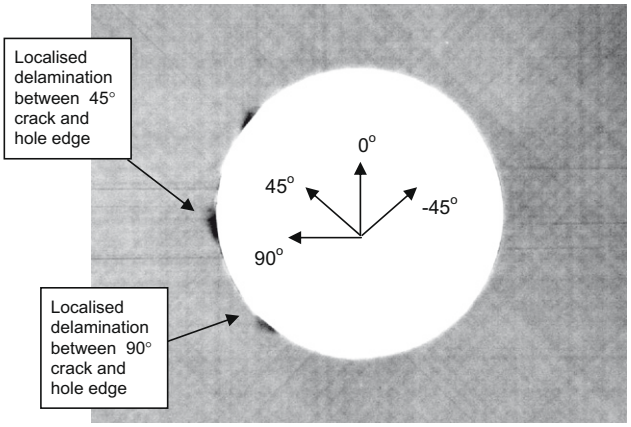

Fig. 4. X-ray image of the damage at the hole of a 4 mm thick ply-level scaled specimen with a 12.7 mm diameter hole at 40% of the expected failure stress (145 MPa).

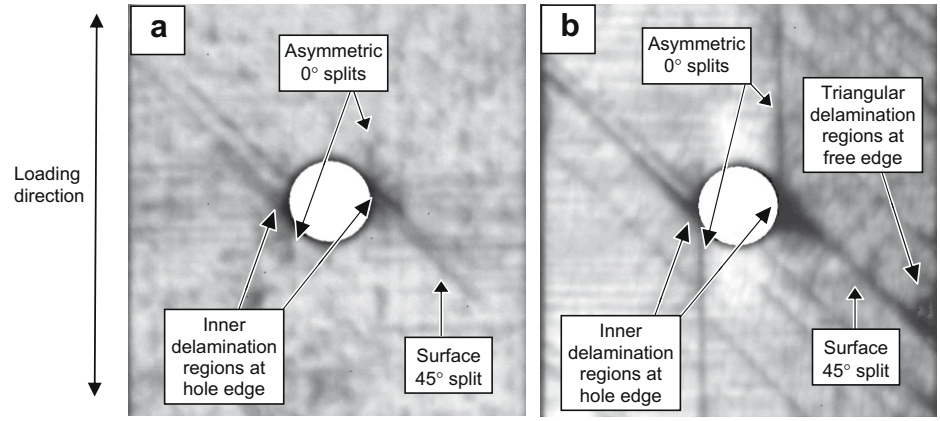

Fig. 5. (a) 4 mm thick ply-level scaled specimen with a 12.7 mm diameter hole C-scan images showing delamination at the hole edge at 60% of failure load (217 MPa) and b) at 95% of failure stress (344 MPa) with 45° splits extended to the free edge and associated delaminations.

one interface to another. Since this delamination is asymmetric with respect to the hole centre due to the adjacent −45° ply, it also led to the asymmetric propagation of 0° splits which can be seen in Fig. 5, for the ply-level scaled specimens. It is the 0° splits that redistribute the stress away from the notch, as described in [18–19], thereby delaying the onset of fibre fracture. The interrupted tests have shown that where the delamination is reduced sufficiently, as was the case in sub-laminate level scaled specimens, the 0° splits will propagate in a symmetric manner, as shown in Fig. 6, which was loaded to 95% of ultimate load. Although there are also matrix cracks visible close to the hole in the off-axis plies, neither the 0° nor off-axis ply damage was present at the lower interrupted load level, thus suggesting that these damage events occurred relatively close together at similar stress levels.

Damage then propagated across the width of the specimen, through the outer delamination regions of Fig. 3 to the specimen edge. The first damage to propagate across the width of the specimen was the main 45° matrix crack from the hole in the surface ply. A small amount of delamination occurred at the intersection of the matrix crack and specimen edge, similar to that which occurred at the hole edge as seen in Fig. 5b. As loading continued, the delaminations at the hole and specimen edge propagated towards each other. When the delaminations became close enough to interact, they joined together to form a delamination across the full width of the specimen. This then is able to propagate via intra-ply matrix cracks, through the thickness of the gauge section. The delaminations remained within the region bounded by the main 45° and −45° matrix cracks which propagated from the hole.

Final catastrophic fibre failure (stage 4) will occur at some point during the sequence of damage described above, with the observed mechanism being determined by the extent of development of the damage mechanisms in stages 1–3 which redistribute the local stresses adjacent to the hole.

5. Finite element model

The experimental results shown in Table 1 have clearly shown the effect of variation of specimen size for 1D, 2D and 3D scaling on strength. A more detailed examination of the failure process has shown the importance of sub-critical damage, which takes the form of intra-ply splitting and inter-ply delamination, on determining the failure mode and hence specimen strength.

In order to capture the size effect for the specimens which failed by the delamination failure mechanism in finite element models it has been found necessary to include the sub-critical damage development in some detail [16]. This is done using cohesive interface elements to account for the intra-ply splitting and inter-ply delamination. For the fibre dominated failure modes a fibre failure criterion is additionally required. For this a statistical criterion based on Weibull theory is used. The splitting and delamination failures influence the fibre directions stress which in turn affects the predicted fibre failure thus explicitly taking account of the damage modes interaction. These failure models are described in more detail below.

5.1. Interface elements

Interface elements based on cohesive zone models are becoming increasingly used for modelling of delamination in composite materials [20–22]. They can also be used for modelling splitting within

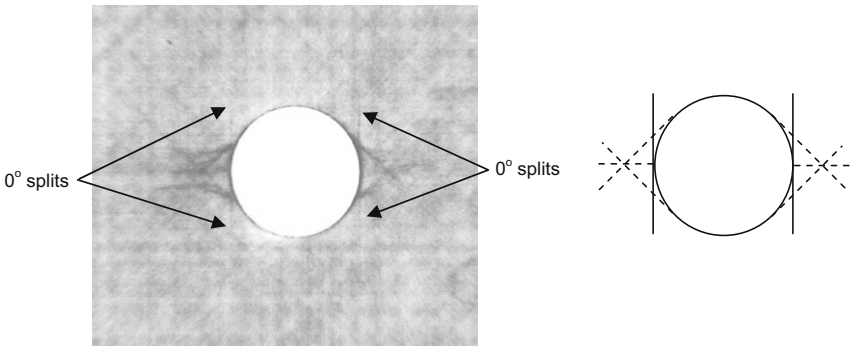

Fig. 6. Symmetric 0° splits in an X-ray of a 4 mm thick sub-laminate level scaled specimen with a 3.175 mm diameter hole having been loaded to 95% of its predicted failure stress (454 MPa).

the plies [11,12]. The interface elements used for this study take the form of discrete elements between initially coincident nodes. Their constitutive behaviour is governed by a bi-linear traction–displacement law. Full details of the formulation are given in a previous publication [16] and so only a brief overview is provided here.

The formulation can be illustrated in a single 3D map, by representing the normal opening mode (mode I) on the 0–σ–δ_{normal} plane, and the transverse shear mode (mode II) on the 0–σ–δ_{shear} plane, as shown in Fig. 7. The triangles 0—$\sigma_I^{\max}$—δ_I^f and 0—$\sigma_{II}^{\max}$—δ_{II}^f are the bilinear responses in the pure opening and pure shear modes respectively [16]. Any point on the 0–δ_{normal}–δ_{shear} plane represents a mixed-mode relative displacement.

The mixed-mode damage onset displacement, δ_m^e, and interfacial strength, $\sigma_m^{\max}$, are calculated using a quadratic damage onset criterion [23]:

$$\sqrt{\left(\frac{\max(\sigma_I, 0)}{\sigma_I^{\max}}\right)^2 + \left(\frac{\sigma_{II}}{\sigma_{II}^{\max}}\right)^2} = 1 \tag{1}$$

The mixed-mode failure displacement corresponding to complete decohesion is calculated using the following power law failure criterion:

$$\left(\frac{G_I}{G_{IC}}\right)^{\alpha} + \left(\frac{G_{II}}{G_{IIC}}\right)^{\alpha} = 1 \tag{2}$$

where $\alpha \in (1.0\text{–}2.0)$ is an empirical parameter derived from mixed-mode tests, G_{IC} and G_{IIC} are critical energy release rates for pure mode I (opening) and pure mode II (shear), respectively, corresponding to the areas under the pure mode traction displacement curves. Eq. (2) allows the fully debonded locus, represented by the relative displacement corresponding to complete interface failure, to be determined (see Fig. 7).

5.2. Fibre failure criterion

In order to predict fibre failure in the laminates a criterion based on Weibull statistics has been used. The decrease in strength with increasing specimen size for brittle-like materials may be well explained using Weibull volumetric statistical strength theory [24–26]. This theory supposes that the strength of a brittle-like material is controlled by flaws which are statistically distributed. The simple two-parameter model states that the probability of survival, P, of a specimen subjected to a stress field σ over a volume V can be represented by Eq. (3),

$$P(\sigma) = \exp\left(-\int_V \left(\frac{\sigma}{\sigma_0}\right)^m dV\right) \tag{3}$$

where σ_0 is the characteristic strength and m the Weibull modulus.

Using the assumption of equal probability of survival at the failure load level, we have:

$$\int_V \left(\frac{\sigma}{\sigma_{unit}}\right)^m dV = 1 \tag{4}$$

where the constant, σ_{unit}, is the unidirectional failure stress of a unit volume of material. Using results from scaled unidirectional tensile tests [27], from a least squares fit of the results from a plot of $\ln\sigma$ vs. $\ln V$, we can derive the material constants as $m = 40.1$ and $\sigma_{\text{unit}} = 3131$ MPa for 1 mm^3. To keep the numerical model simple, instead of incorporating the fibre failure criterion directly in the finite element material model, a sequential checking of the Weibull failure criterion through the loading history has been performed in a post-processing routine. The 0° ply fibre direction stresses at each load increment are integrated and checked against the criterion. The integration in the failure criterion becomes a summation over all the elements in the finite element model, using the stress at the centroid of each element.

$$\int_V \left(\frac{\sigma}{\sigma_{unit}}\right)^m dV = \sum_{i=1}^{\text{Total No of Solid Elements}} \left(\frac{\sigma_i}{\sigma_{unit}}\right)^m V_i \geqslant 1 \tag{5}$$

The predicted fibre failure stress level can be taken to be the loading point where the criterion is first met.

5.3. Open hole tension model details

Models of the open hole tensile tests were created in the explicit finite element code LS-Dyna. The cohesive interface element described in Section 5.1 has been embedded as a user material. Fig. 8 shows a typical mesh created from fully integrated solid elements and also the location where interface elements were inserted. In all cases a single element was used through the thickness of each ply block. Although this is not sufficient to capture the case of a tunnelling crack, the modelling of matrix cracks here is important only in so far as they are related to the delaminations. Previous work [16] has indicated that this is sufficient to achieve a satisfactory solution which is not sensitive to the number of elements through the thickness in this case. The in-plane mesh was refined such that a converged solution was also obtained. The element in-plane size

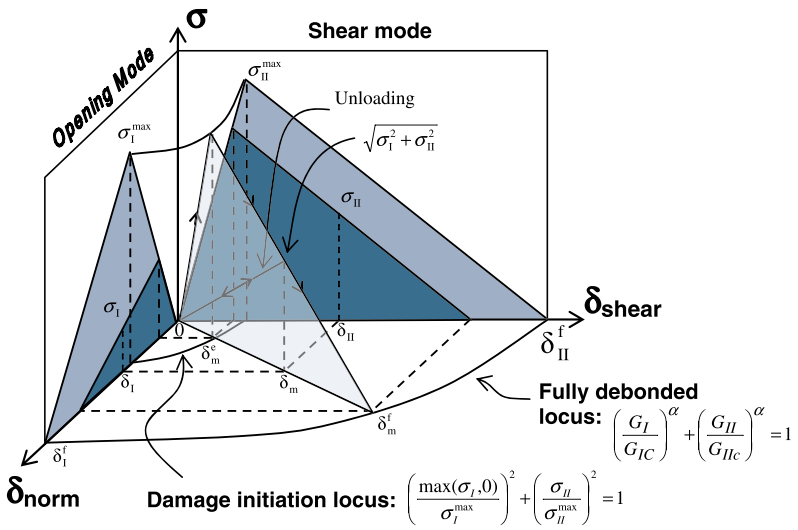

Fig. 7. Mixed-mode traction displacement relationship for interface elements [16].

was kept approximately constant in the critical regions (about one to two ply thicknesses, ~0.125–0.25 mm) as the model dimensions were increased in size for the scaled specimens. This is necessary in order to preserve a sufficient number of interface elements in the process zone ahead of a predicted crack tip, see [28] for further details. A half model through the thickness was used due to the symmetry of the layup. Interface elements were inserted between each ply block to predict the delamination. Also at selected locations within each ply block, lines of interface elements were inserted to model the intra-ply splitting (matrix cracking). From the experimental programme it was observed that the major splits occur starting tangential from the hole edge, propagating in the fibre direction of each ply. In the case of the 90° ply, the split was inserted at the point of maximum stress concentration. Inserting these lines within the ply mesh resulted in small degenerated elements around the hole which were removed, resulting in a slightly misshapen hole. Although this will effect the linear elastic stress concentration, once the splitting initiates (as it does in all cases examined here) the stress concentration is relieved and the exact geometry of the hole does not affect results. Thermal residual stresses were included in the model by applying a −160 °C temperature reduction prior to mechanical loading to simulate cool down from the 180 °C processing temperature to a room temperature of 20 °C. Mechanical loading was applied using a prescribed displacement on the nodes at the end of the gauge section at a rate sufficiently slowly so as not to induce dynamic effects. The material properties used for the plies were obtained from [29] and the interface element fracture properties from a best fit to experimental data from [30]. For the interface element maximum stresses, typical values for epoxy matrix material were used. Since it is the propagation of the matrix cracks and delaminations that are the significant events, rather than their initiation, the exact value used for these latter parameters is not critical. These input properties are summarised in Table 3.

Table 3
Material properties used in finite element models.

IM7/8552 individual ply properties (1 = fibre direction)							
E_{11}	$E_{22} = E_{33}$	$G_{12} = G_{13}$	G_{23}	$\nu_{12} = \nu_{13}$	ν_{23}	α_{11}	$\alpha_{22} = \alpha_{33}$
161 GPa	11.4 GPa	5.17 GPa	3.98 GPa	0.32	0.436	0.0 °C^{-1}	3×10^{-5} °C^{-1}
Interface element properties							
G_{IC}		G_{IIC}		α		σ_I^{max}	σ_{II}^{max}
0.2 N/mm		1.0 N/mm		1.0		60 MPa	90 MPa

5.4. Results and determination of failure mode

After the initial thermal loading, the increasing mechanical load eventually starts to induce damage in the specimens through failure of the interface elements. Fig. 9 shows a typical sequence of the damage development, in this case for the 4 mm thick, ply-level scaled specimen with a 25.4 mm diameter hole. Each row shows a plan view of the specimen with the predicted damage at an increasing applied displacement. The far field stress is calculated from the nodal reaction forces. Predicted delamination at each of the three interfaces is shown separately. The coloured areas indicate completely failed interface elements. In areas far away from the hole this can appear as a series of lines or points instead of continuous colour due to the coarser mesh used in these areas. The predicted splitting in all plies is shown simultaneously in a single image at each load on the right hand side. The sequence of damage development is discussed in some detail in the following sections, here it is sufficient to note the significant delamination that propagates back towards the ends of the specimen at the −45/0 interface. Just prior to this is the point of maximum stress before a significant drop on the load displacement curve.

This load drop signifies the point of delamination failure. All of the analyses conducted predicted this delamination failure point eventually since there was no fibre failure embedded in the numerical analysis. The point of fibre failure was predicted by post-processing the analysis results using the Weibull based criterion described in Section 5.2. Comparison of the relative position of these two events on the load–displacement curve has enabled the analysis to be used to predict the specimen failure mode (see Fig. 10). If the Weibull failure criterion was only satisfied after the point at which the delamination caused the significant load drop then it was classified as a delamination failure. If the Weibull criterion was satisfied before the load had reduced then it was classified as a fibre failure. It was not possible to discriminate between the pull-out and brittle fibre dominated failure modes shown in Fig. 1 from the analysis. The specimens from the scaled testing programme shown in Table 1 [15] were modelled using the method described here. In each case a failure stress and failure mode could be predicted. The results are summarised in Table 4.

6. Experimental vs. modelling comparison

The comparison between the experimental and modelling work has shown a very good correlation for predicted strength and failure mechanism, helping to explain the size effect observed in notched composites, and giving confidence in the use of the combined Weibull criterion and cohesive interface element technique for detailed composite behaviour prediction.

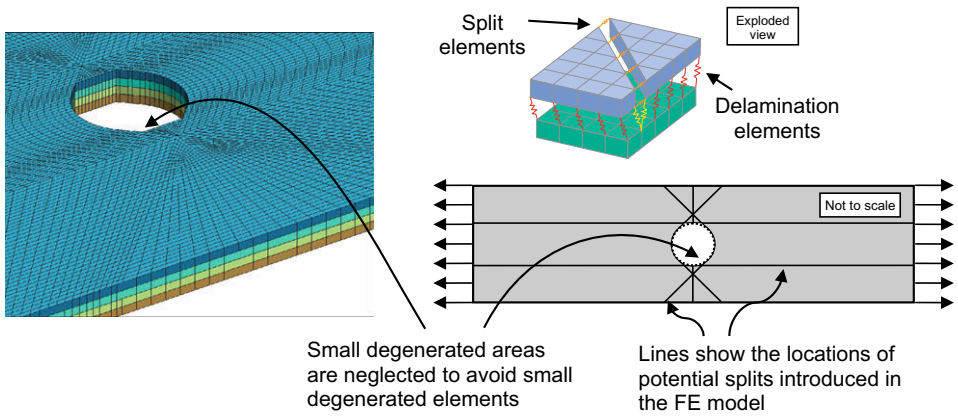

Fig. 8. Typical mesh (2 mm thick, ply scaled specimen) and location where interface elements were inserted.

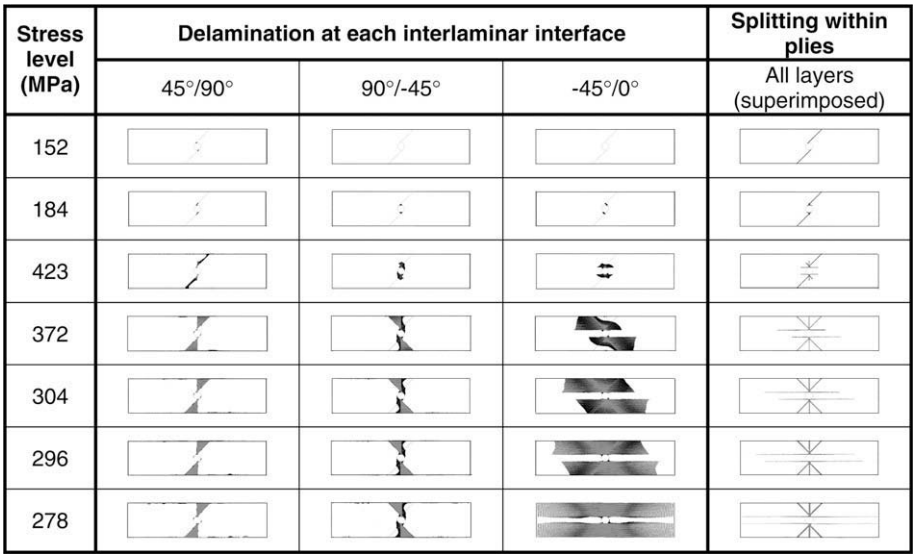

Fig. 9. Typical damage development in FE model at the different interfaces (4 mm thick ply-level scaled specimen with a 25.4 mm diameter hole).

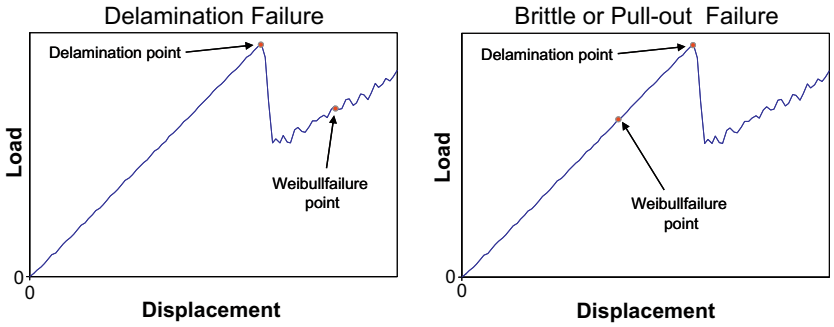

Fig. 10. Determination of the failure mode from the load/displacement curves.

Table 4
Finite element predictions for the scaled open hole tensile tests presented in [15].

Laminate thickness t (mm)	Hole sizes (mm)							
	Sub-laminate level scaling				Ply-level scaling			
	3.175	6.35	12.7	25.4	3.175	6.35	12.7	25.4
1	**630**				**630**			
2	**498**	**460**			*434*	*514*		
4	**498**	**463**	**424**	**364**	*239*	*301*	*362*	*423*
8	**499**			**368**	*178*			*246*

Bold font values indicate brittle or pull-out and italicized values indicate delamination type failures.

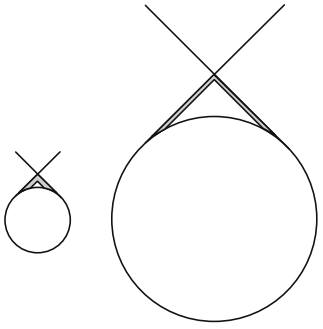

Fig. 11. Relative size of delamination at the hole edge compared with hole size.

6.1. Ply-level scaled specimens

6.1.1. Damage development

Damage development in the ply-level scaled specimens correlated very well between experimental and modelling work in terms of the damage patterns, the order in which damage occurred, and extent to which it grew. The different stress at which the delamination propagated back to the grips was controlled by the development of damage at the hole edge and its propagation across the width of the specimen. This in turn is controlled by the ply block thickness and ligament width, which is related to hole diameter in these scaled specimens. Localised delamination at the hole occurred earlier for a smaller diameter, as seen in the experimental investigation, because the initial cracking and delamination can join up more easily due to the smaller distances between the individual failures [31]. Since the size of the delaminations associated with the intersection of matrix cracks and free edges is dependent on ply thickness, it is easier for the delaminations to join up for small hole sizes at constant ply block thickness, see Fig. 11. Damage thus propagated through the thickness of the laminate at a lower stress for the smaller hole diameter.

As well as splitting in the off axis plies, splitting also occurs in the 0° plies. Since the damage propagation is dependent on the local delamination at the hole and the way in which it follows the ply orientation through the thickness of the laminate, the 0° splits

develop asymmetrically. The analysis correctly predicted the development of these splits, including the asymmetry. Fig. 12 shows the difference between the 0° splitting pattern of 4 mm thick specimens with 3.175 and 12.7 mm diameter holes, comparing the experimental results at 80% of their respective average failure loads with modelling results, at 80% of the predicted failure load. In both the experimental and modelling cases, the asymmetric splitting pattern is more pronounced for the smaller hole diameter; for the larger hole diameter, the increase in failure stress (due to reduced damage) means that splitting occurs in all four quadrants of the specimen, becoming more symmetric. The experimental results also show a number of other cracks which were not modelled, but do not appear to affect the overall behaviour because they do not interact with the stress concentration at the hole.

When the initial 45° matrix crack reached the specimen edge, it induced a small area of delamination, as also seen initially at the hole edge. For a smaller hole diameter (and therefore specimen width in this case), the delamination at the specimen edge is relatively larger than for a larger hole diameter, allowing it to more easily propagate across the width of the specimen, leading to a lower failure stress. Fig. 13 shows the delamination at the 45/90 interface from the analyses of the 4 mm thick ply-level scaled specimens with a 3.175 and 12.7 mm diameter hole at 95% of their respective failure loads. The specimen with the 12.7 mm diameter hole (central image) however requires a considerably higher load to achieve what is a larger delamination area. It can be seen that the damage patterns are very similar and compare well with Fig. 5b. The right hand image shows a 2 mm thick ply-level scaled specimen with a 3.175 mm hole which has a reduced level of damage when compared to the 4 mm thick specimen at the same diameter and percentage of failure load (left hand image). This is a result of the smaller ply thickness to hole diameter ratio.

6.1.2. Failure stress and mechanism

All of the ply-level scaled specimens with the exception of the very smallest were predicted to fail by the delamination failure mode. In all cases the analysis was able to correctly predict the failure mode with the exception of the 2 mm thick specimen with a

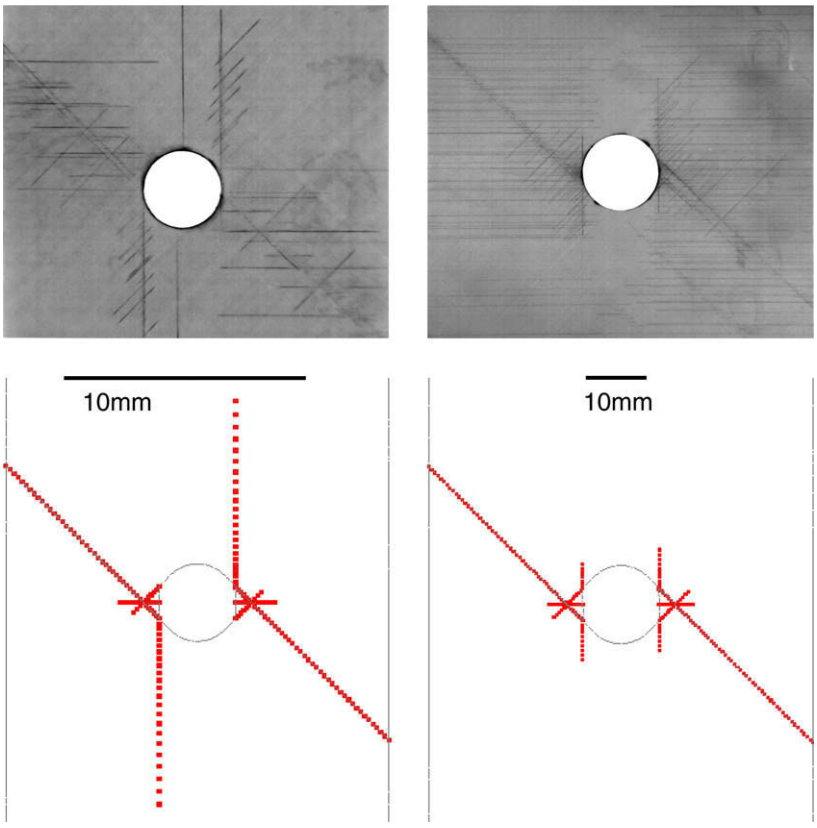

Fig. 12. X-ray and finite element split predictions for 4 mm thick ply-level scaled laminate with 3.175 mm (left) and 12.7 mm (right) holes loaded to 80% of their failure loads. FE plots are at 80% of the predicted failure load.

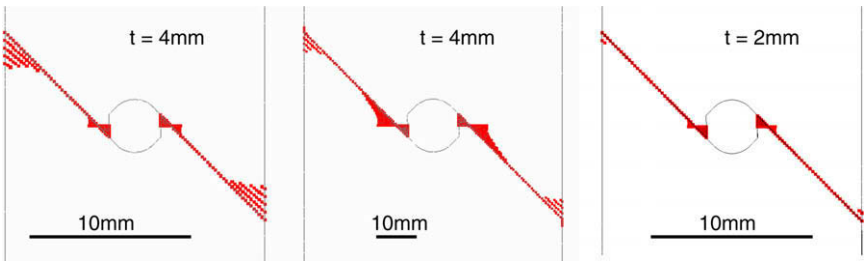

Fig. 13. Finite element models of 4 mm ply-level scaled specimens with 3.175 mm (left) and 12.7 mm (centre) diameter holes and 2 mm ply-level scaled 3.175 mm diameter hole specimen (right) showing 45/90 delamination and 45 ply split, all at 95% of their predicted failure load.

6.35 mm diameter hole which was classified overall as pull-out in the experimental work. These specimens in fact also showed some delamination failures in a minority of tests, thus indicating that it is at the transition point between the two modes. The point at which delamination occurs is characterised by a distinctive drop in load. Fig. 14a shows a typical experimental curve from 4 mm thick specimens with 3.175 and 25.4 mm hole diameters and Fig. 14b the respective analyses. It is not meaningful to compare displacements directly as in the experimental case only cross-head displacements were measured which includes any machine compliance and grip deformation and slippage.

It can be seen that the graph for the smaller hole diameter has two distinctive load drops. This is as a result of the asymmetric damage development which was seen in Fig. 12. This asymmetry is continued with the propagation of delamination at the 45/0 interface, first on one side of the specimen, causing the first load drop and then on the other side, causing the second load drop. This behaviour is captured well by the analysis which also shows two peaks for the smaller specimen and a single peak for the larger 25.4 mm diameter hole specimen in which the 45/0 delamination propagated symmetrically across the entire gauge section of the laminate. Fig. 15 shows an X-ray of a 4 mm ply-level scaled specimen with a 3.175 mm diameter hole from the interrupted tests after the first load drop. From the pattern of the zinc iodide penetrant the area of delamination can be clearly observed to be asymmetric. The analysis from a similar point on the load curve can be seen to show a very similar pattern of delamination.

Fig. 16 shows a comparison of the experimental failure stresses compared with the predicted numerical results for thickness only scaling (1D), in-plane only (2D) and full 3D scaling. It can be seen that an extremely good level of correlation has been achieved, capturing both the individual quantitative failure stress results and the overall trends. This includes that of the increasing strength for the in-plane scaling which can be explained in terms of the sub-critical damage development described above. Indeed it is only through the detailed modelling of the sequence of significant sub-critical damage events that such a robust and accurate predictive model can be created. This has been achieved using only independently measured material properties without the need for any further fitting parameters.

6.2. Sub-laminate level scaled specimens

6.2.1. Damage development and stress–displacement curve

For the sub-laminate-level scaled specimens damage follows the same general trend as described in Section 4. However in this case the development of the sub-critical damage is not as extensive as that observed in the ply-level scaled specimens and in all cases the specimens failed by either the pull out or brittle failure modes. Two effects delay the onset of the local delamination at the hole edge. Firstly, the thinner plies compared to the ply-level scaled

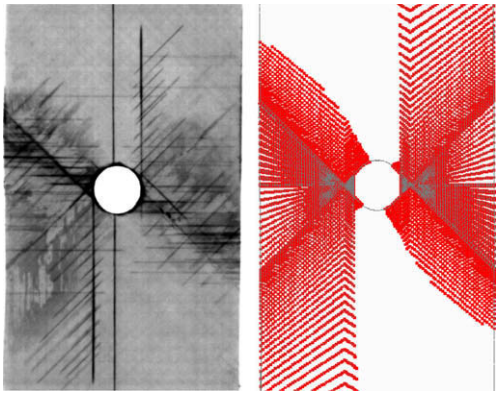

Fig. 15. X-ray of 4 mm ply-level scaled specimen with a 3.175 mm diameter hole after first load drop and predicted delamination at all interfaces, also after the first load drop.

specimens mean that the propensity to delaminate at the hole edge is reduced for a given hole diameter. Secondly, damage occurs predominantly in the outermost sub-laminates because the outermost 0° plies interrupt the propagation of damage through the thickness of the laminate. Fig. 17 shows a plot of the 2 mm sub-laminate level scaled specimen with a 3.175 mm diameter hole at the predicted fibre failure stress (498 MPa). Each row represents the interfaces within a quasi-isotropic 45/90/ − 45/0 sub-laminate as well as the splitting within each sub-laminate block superimposed. There is a very small amount of delamination and splitting at the hole edge, restricted to the inner delamination area. It can be seen that the damage is restricted to the first sub-laminate from the surface for delamination and that the inner sub-laminate sustains only a reduced amount of intra-ply splitting damage. This level of damage is generally consistent with the X-ray of the test of this configuration, interrupted at 95% of ultimate load shown in Fig. 6, except for the 0° splitting. The lack of 0° splitting in Fig. 17 when compared to Fig. 6 may be accounted for by the softening zone (i.e. interface elements which have initiated damage but not yet reached complete failure) that develops ahead of the fully failed interface elements and is not shown in the analysis figures. In the case of mode II loading, which is predominant in the 0° splits, the length of this softening zone can be quite significant (up to 4 mm [28]). This pattern of damage occurring only in the surface sub-laminate is continued to the thicker laminates which contain more sub-laminates but no further damage. This can explain why there is no further strength reduction with increasing thickness.

The limited amount of damage observed occurs at a lower stress for a smaller hole diameter. The stress relieving 0° splits are also relatively longer for a smaller hole diameter, thus delaying fibre failure and increasing specimen strength. This can be seen by comparing the relative splits length seen in Fig. 18 with those in Fig. 6.

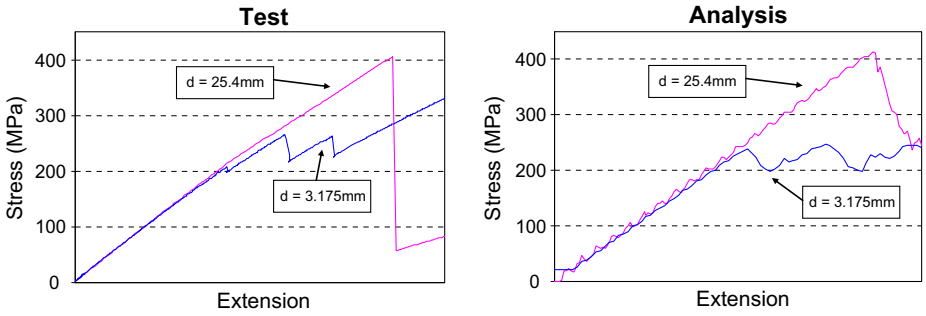

Fig. 14. Typical stress-extension curves for 4 mm thick ply-level scaled tests with 3.175 and 25.4 mm hole diameters.

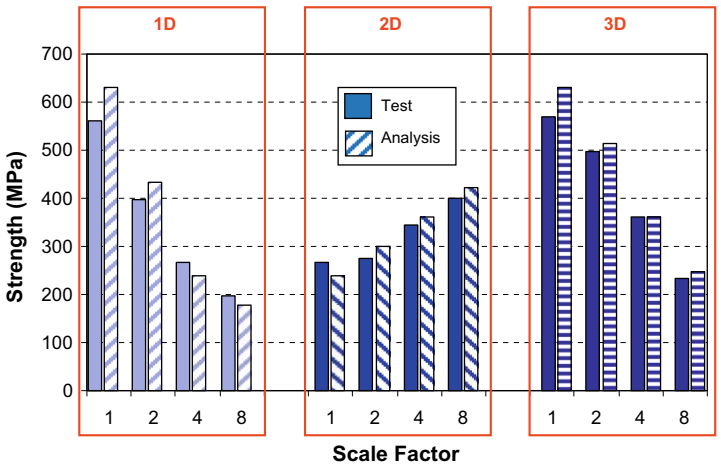

Fig. 16. Comparison of experimental to analysis results for ply-level 1D, 2D and 3D scaling.

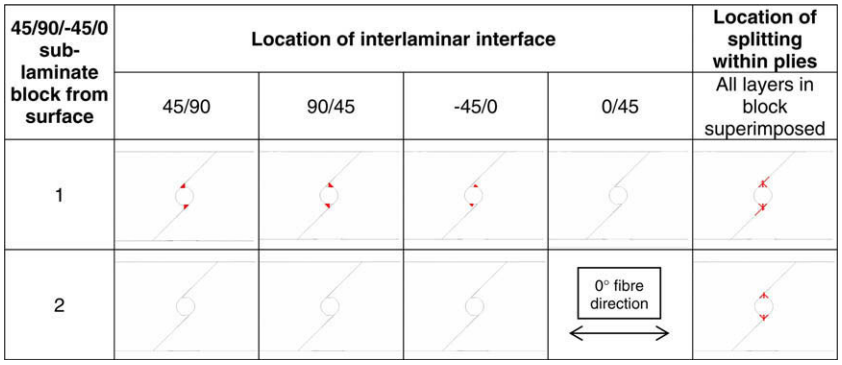

Fig. 17. Sub-critical damage development in 2 mm thick sub-laminate level scaled specimen with 3.175 mm diameter hole at predicted fibre failure stress (498 MPa).

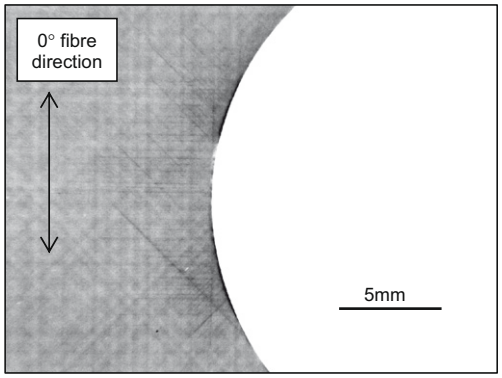

Fig. 18. Damage development in a 4 mm thick sub-laminate level scaled specimen with a 25.4 mm diameter hole having been loaded to 95% of failure load (314 MPa).

6.2.2. Failure stress and mechanism

The load–displacement curves from the experimental programme were all quite linear to failure. This was also the case for the analysis which showed relatively little sub-critical damage prior to failure. In all cases the analysis predicted a fibre failure prior to delamination. It was not possible to discriminate between the pull-out and brittle failure modes from the analysis. It was however notable that for those configurations which exhibited a brittle failure experimentally, the analysis predicted the fibre failure to occur at a lower percentage of the predicted delamination stress (<50%) than those that failed by pull-out (>50% of delamination stress). As with the ply-level scaling a good level of correlation between the experimental and analysis results was obtained (Fig. 19), both for the individual quantitative results and the overall trends.

6.3. Discussion

The difference in the tensile strength scaling effect between the ply-level and sub-laminate level scaled specimens investigated can be summed up as follows. In all cases delamination at the hole, which allows damage to propagate through the thickness of the laminate, occurs at a lower stress for a smaller hole diameter (for a constant ply thickness). For the majority of ply-level scaled specimens, this damage leads to delamination at the −45/0 interface which is the ultimate failure mechanism. This results in an increasing failure stress with increasing hole diameter. In contrast for sub-laminate level scaled specimens, the reduction in the propagation of damage through the gauge section with increasing hole diameter reduced the amount of stress relief present and led to earlier fibre failure. The analysis method presented here has been able to capture each of these detailed mechanisms in turn and thus been able to predict all of the experimentally observed trends in scaling by changing thickness, in-plane dimensions and full 3D scaling for both ply and sub-laminate level scaling.

7. Conclusions

Interrupted testing on carbon fibre/epoxy laminates containing a circular hole has identified the damage progression within the specimens as load is increased. Firstly, damage occurs at the hole

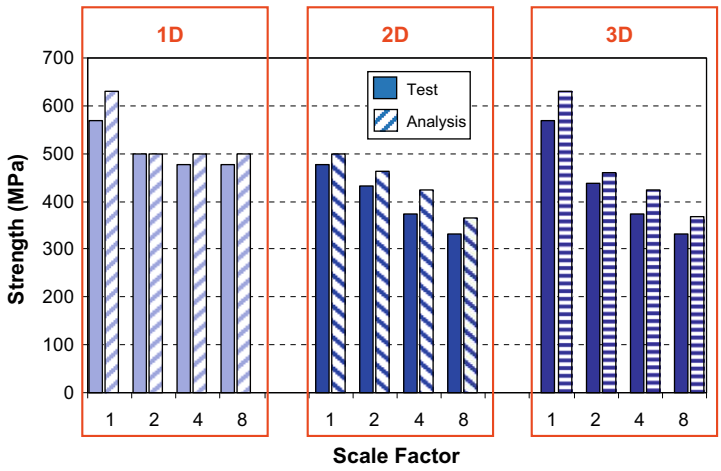

Fig. 19. Comparison of experimental to analysis results for sub-laminate level 1D, 2D and 3D scaling.

edge, in the form of matrix cracking in the off-axis plies, with associated delaminations. This is followed by more extensive damage at the hole edge in the form of larger areas of delamination between plies, which in turn allows the damage to propagate through the thickness of the laminate and provides stress relaxation by splitting in the 0° plies. Finally, damage occurs throughout the gauge section, away from the influence of the stress concentration induced by the hole. Fibre failure will occur at some point during this sequence, dependent on the relative 0° fibre stress and the extent of the delamination.

The damage sequence and pattern observed experimentally correlated excellently with that predicted by an FE model using interface elements to model splitting and delamination propagation, and a Weibull based statistical analysis for fibre failure. The stress level at which the load drops occurred, caused by delamination failure also showed excellent correlation as did the predicted fibre failure stress. The overall trends of the different scaling regimes were therefore well captured by the model. These predictions were all produced using independently measured material data with no further fitting parameters.

A combination of the experimental and FE results was able to explain the size effect in composite laminates containing circular holes reported in previous work, looking at both ply- and sub-laminate level scaled specimens. In both cases, the crucial damage event is localised delamination at the hole edge. This was seen to occur at a lower stress for a smaller hole diameter. For ply-level scaled specimens, this allowed damage to propagate through the thickness of the laminate at a lower stress for a smaller hole diameter, leading to an earlier delamination failure (or an increasing failure stress for increasing hole diameter). For sub-laminate level scaled specimens, damage was constrained to the outermost sub-laminate, inhibiting its propagation through the thickness of the laminate, thus leading to a fibre failure. Small amounts of damage still propagated at a lower stress for a smaller hole diameter, leading to greater stress relief for a smaller hole. Thus as hole diameter increased, specimen strength decreased. By the means described above, ply and laminate thickness, and hole diameter, control the extent to which damage grows in the laminate, and hence the failure stress and mechanism, leading to the previously observed size effect.

Acknowledgements

The authors acknowledge the support of Airbus UK, the Engineering and Physical Sciences Research Council, MoD and Hexcel for their support of this work. Thanks also to Xiangqian Li at the University of Bristol for help in completing the very large sub-laminate level scaled analyses.

References

[1] Spearing SM, Lagace PA, McManus HLN. On the role of lengthscale in the prediction of failure of composite structures: assessment and needs. Appl Compos Mater 1998;5(3):139–49.
[2] Awerbuch J, Madhukar MS. Notched strength of composite laminates: predictions and experiments – a review. J Reinforced Plastics Compos 1985;4(1):3–159.
[3] Whitney JM, Nuismer RJ. Stress fracture criteria for laminated composites containing stress-concentrations. J Compos Mater 1974;8:253–65.
[4] Chang FK, Chang KY. A progressive damage model for laminated composites containing stress-concentrations. J Compos Mater 1987;21(9):834–55.
[5] Kortschot MT, Beaumont PWR. Damage mechanics of composite-materials. 2. A damaged-based notched strength model. Compos Sci Technol 1990;39(4):303–26.
[6] Kortschot MT, Beaumont PWR. Damage mechanics of composite-materials. 1. Measurements of damage and strength. Compos Sci Technol 1990;39(4):289–301.
[7] Kortschot MT, Beaumont PWR, Ashby MF. Damage mechanics of composite-materials. 3. Prediction of damage growth and notched strength. Compos Sci Technol 1991;40(2):147–65.
[8] Hallett SR, Wisnom MR. Experimental investigation of progressive damage and the effect of layup in notched tensile tests. J Compos Mater 2006;40(2):119–41.
[9] Coats TW, Harris CE. A progressive damage methodology for residual strength predictions of notched composite panels. J Compos Mater 1999;33(23):2193–224.
[10] Camanho PP, Maimi P, Davila CG. Prediction of size effects in notched laminates using continuum damage mechanics. Compos Sci Technol 2007;67(13):2715–27.
[11] Wisnom MR, Chang FK. Modelling of splitting and delamination in notched cross-ply laminates. Compos Sci Technol 2000;60(15):2849–56.
[12] Hallett SR, Wisnom MR. Numerical investigation of progressive damage and the effect of layup in notched tensile tests. J Compos Mater 2006;40(14):1229–45.
[13] Kwon YW, Craugh LE. Progressive failure modeling in notched cross-ply fibrous composites. Appl Compos Mater 2001;8(1):63–74.
[14] Yang QD, Cox B. Cohesive models for damage evolution in laminated composites. Int J Fract 2005;133(2):107–37.
[15] Green BG, Wisnom MR, Hallett SR. An experimental investigation into the tensile strength scaling of notched composites. Compos Part A – Appl S 2007;38(3):867–78.
[16] Jiang WG, Hallett SR, Green BG, Wisnom MR. A concise interface constitutive law for analysis of delamination and splitting in composite materials and its application to scaled notched tensile specimens. Int J Numer Meth Eng 2007;69(9):1982–95.
[17] Salpekar SA, Obrien TK. Analysis of matrix cracking and local delamination in (O/Theta/-Theta)S graphite-epoxy laminates under tensile load. J Compos Tech Res 1993;15(2):95–100.
[18] Mollenhauer D, Iarve EV, Kim R, Langley B. Examination of ply cracking in composite laminates with open holes: a moire interferometric and numerical study. Compos Part A – Appl S 2006;37(2):282–94.
[19] Kortschot M, Beaumont P. Damage-based notched strength modeling: a summary. In: T. O'Brien, editor. Composite materials: fatigue and fracture (vol. 3), ASTM STP 1110. Philadelphia: American Society for Testing and Materials; 1991. p. 596–616.

[20] Hallett SR. Predicting progressive delamination via interface elements. In: Sridharan S, editor. Delamination behaviour of composites. Woodhead; 2008.
[21] Pinho ST, Iannucci L, Robinson P. Formulation and implementation of decohesion elements in an explicit finite element code. Compos Part – Appl S 2006;37(5):778–89.
[22] Camanho PP, Davila CG, de Moura MF. Numerical simulation of mixed-mode progressive delamination in composite materials. J Compos Mater 2003;37(16):1415–38.
[23] Brewer JC, Lagace PA. Quadratic stress criterion for initiation of delamination. J Compos Mater 1988;22(12):1141–55.
[24] Wisnom MR. Relationship between strength variability and size effect in unidirectional carbon–fiber epoxy. Composites 1991;22(1):47–52.
[25] Wisnom MR, Atkinson JW. Reduction in tensile and flexural strength of unidirectional glass–fibre epoxy with increasing specimen size. Compos Struct 1997;38(1–4):405–11.
[26] Wisnom MR. The relationship between tensile and flexural strength of unidirectional composites. J Compos Mater 1992;26(8):1173–80.
[27] Wisnom MR, Khan B, Hallett SR. Size effects in unnotched tensile strength of unidirectional and quasi-isotropic carbon/epoxy composites. Compos Struct 2008;84(1):21–8.
[28] Harper PW, Hallett SR. Cohesive zone length in numerical simulations of composite delamination. Eng Fract Mech 2008;75(16):4774–92.
[29] O'Brien TK, Krueger R. Analysis of ninety degree flexure tests for characterization of composite transverse tensile strength. NASA TM-2001-211227 ARL-TR-2568, 2001.
[30] Jimenez MA, Miravete A. Application of the finite-element method to predict the onset of delamination growth. J Compos Mater 2004;38(15):1309–35.
[31] Wisnom MR, Hallett SR. The role of delamination in strength, failure mechanism and hole size effect in open hole tensile tests. Compos Part A – Appl S 2009;40(4):335–42.